

# Cosmological perturbations in an effective and genuinely phantom dark energy Universe

Imanol Albaran <sup>1,2,a</sup> Mariam Bouhmadi-López <sup>1,2,3,4,b</sup> and João Morais <sup>3c</sup>

<sup>1</sup>*Departamento de Física, Universidade da Beira Interior,*

*Rua Marquês D'Ávila e Bolama 6200-001 Covilhã, Portugal*

<sup>2</sup>*Centro de Matemática e Aplicações da Universidade da Beira Interior,*

*Rua Marquês D'Ávila e Bolama 6200-001 Covilhã, Portugal*

<sup>3</sup>*Department of Theoretical Physics University of the Basque Country UPV/EHU. P.O. Box 644, 48080 Bilbao, Spain*

<sup>4</sup>*IKERBASQUE, Basque Foundation for Science, 48011, Bilbao, Spain*

(Dated: May 8, 2019)

We carry out an analysis of the cosmological perturbations in general relativity for three different models which are good candidates to describe the current acceleration of the Universe. These three set-ups are described classically by perfect fluids with a phantom nature and represent deviations from the most widely accepted  $\Lambda$ CDM model. In addition, each of the models under study induce different future singularities or abrupt events known as (i) Big Rip, (ii) Little Rip and (iii) Little Sibling of the Big Rip. Only the first one is regarded as a true singularity since it occurs at a finite cosmic time. For this reason, we refer to the others as abrupt events. With the aim to find possible footprints of this scenario in the Universe matter distribution, we not only obtain the evolution of the cosmological scalar perturbations but also calculate the matter power spectrum for each model. Finally, we constrain observationally these models using several measurements of the growth rate function, more precisely  $f\sigma_8$ , and compare our results with the observational ones reaching the conclusion that even if these three models are very similar at present there are small differences that could allow us to distinguish them.

Keywords: Dark energy, cosmological perturbations, cosmic singularities, large scale structure.

---

<sup>a</sup> imanol@ubi.pt

<sup>b</sup> mbl@ubi.pt , (On leave of absence from UPV and IKERBASQUE)

<sup>c</sup> jviegas001@ikasle.ehu.eus

## I. INTRODUCTION

Cosmology has made a long way on the last years with the impressive amount of observations and theoretical advancements. Yet, cosmology faces many challenging questions like the fundamental cause of the recent acceleration of the Universe as predicted by SNeIa observations almost twenty years ago [1, 2], and afterwards confirmed by several type of cosmological and astrophysical observations (see for example [3] for a recent account on this issue). The simplest approach is to assume a cosmological constant that started recently dominating the late-time energy density budget of the Universe which is in agreement with the current observations [4]. But then the issues *of why is it so tiny?* and *why this cosmological constant has begun to be important only right now?* have to be addressed as well (see for example: [5–8]). Another, equally important, issue is what happens if the cosmological constant is not quite constant? This has lead to a great interest in exploring other possible scenarios to explain the late-time acceleration of the cosmos by invoking either an additional matter component in the Universe, which we name dark energy (DE) [9–11], or by modifying appropriately the laws of gravity (for a recent account on this issue see, for example, [12, 13] and the extensive list of references provided therein).

We will focus on the third question: *what happens if the cosmological constant is not quite constant?* More precisely, we will address this question on the framework of the cosmological perturbations and for some DE models whose equations of state; i.e., the ratio between its pressure and its energy density, deviate slightly from the one corresponding to a cosmological constant. Before proceeding let us remind the following well known fact: if the equation of state (EoS) of DE deviates from -1, the Universe fate might be quite different from the one corresponding to an empty de Sitter Universe. In particular, if the equation of state of dark energy is smaller than -1, i.e., DE is apparently (and at least from an effective point of view) not fulfilling the null energy condition, several future singularities or abrupt events might correspond to the cosmic doomsday of the Universe. Amazingly, some of these models are in accordance with current data [14].

On the other hand, the theory of cosmological perturbations is a cornerstone of nowadays cosmology. It provides us with a theoretical framework which allows us to determine, for example, the CMB predicted from an early inflationary era or compute the matter power spectrum and the growth rate of matter in order to make a comparison with the observational results. In addition, it allows us to compute the evolution and possible clustering of DE perturbations and investigate their effect on the growth of dark matter (DM). Even though no perturbations of DE have so far been detected, and are in fact absent in the  $\Lambda$ CDM model, the existence of a great number of experiments aiming to probe the physics of the late-Universe, like the Dark Energy Survey [15] and the Euclid mission [16], suggests that a thorough study and characterization of such effects can be proven to be important to understand the nature of this mysterious fluid that drives the acceleration of the Universe. With this mindset, on this work we analyse the perturbative effects of phantom DE models and look for observational fingerprints that could be used as a mean to favour or disregard such models.

There are three genuinely phantom DE fates; i.e., which happens if and only if a phantom DE component is present:

- Big Rip (BR) singularity: It happens at a finite cosmic time with an infinite scale factor where the Hubble parameter and its cosmic time derivative diverge [17–24].
- Little Rip (LR): This case corresponds to an abrupt event, i.e., it is not strictly speaking a future space-time singularity, as it takes place at an infinite cosmic time [25]. The radius of the Universe, the Hubble parameter and its cosmic time derivative all diverge at an infinite cosmic time [25–32].
- Little Sibling of the Big Rip (LSBR): This behaviour again corresponds to an abrupt event rather than a future space-time singularity. At this event, the Hubble rate and the scale factor blow up but the cosmic derivative of the Hubble rate does not [33, 34]. Consequently, this abrupt event takes place at an infinite cosmic time where the scalar curvature diverges.

These three cases share in common the fact that in the (far) future all the structures in the Universe would be ripped apart in a finite cosmic time [31, 33]. The classical singular asymptotic behaviour of these dark energy models has lead to a quantum cosmological analysis of these setups [35–39]. In these works, it was concluded that once the Universe enters in a genuinely quantum phase; i.e., where coherence and entanglement effects are important, the Universe would evade a doomsday *à la rip* and this applies even to the smoother version of these singular behaviours corresponding to a LSBR [38] (see also [40–44]).

In this paper, we will analyse the cosmological perturbations of DE models that induces a BR, LR or LSBR. While the background analysis of the phantom DE scenario has been widely analysed this has not been the case of its cosmological perturbations [45–49]. In [46, 48, 49] a kinematical approach was assumed, i.e., a dependence of the scale factor as a function of the cosmic time was considered for FLRW Universes with future singularities at a finite cosmic time. Within this setup and using approximated equations for the growth of the perturbations at late-time,

the authors obtained the DM and DE perturbations [48]. Furthermore, in [46, 49], DE perturbations are disregarded and only the growth rate of matter perturbations is calculated. In this work, we will rather assume a dynamical model, i.e., we assume a given EoS for DE. This is the approach employed in Ref [47], where the future behaviour of the linear scalar perturbations is presented for a type of model that, depending on the value of the parameters, can lead to a BR or a Big freeze singularity [50]. In our analysis, we use the full theory of linear perturbation to study how the perturbations of DM and DE, as well as the gravitational potential, evolve for a range of different scales. Our numerical integrations start from well inside the radiation era and continue till the far future. In fact, in order to see the behaviour of the phantom DE models, we extend our numerical calculations till the Universe is roughly  $e^5$  times larger than at present, i.e., roughly  $z \sim -0.99$ .

The paper is organised as follows: In Sect. II, we briefly review DE models that induce a BR, LR or LSBR; i.e., we review perfect fluid that can describe DE from a phenomenological point of view and leading to the above mentioned singularity or abrupt events. In Sect. III, we present the framework for studying the scalar linear perturbations. The evolution equations obtained employ no approximations and are therefore valid for all relevant modes and redshifts, as long as the linear theory is itself valid. A phenomenological mapping of the DE fluid to a phantom scalar field is employed to avoid classical instabilities in the perturbations of DE. We present our numerical results in Sect. IV, where we show the evolution of different perturbed quantities related to DM and DE. We present as well the matter power spectrum for the different models. We equally constrain these models using several measurements of the growth rate function, more precisely  $f\sigma_8$ . Finally, in Sect. V, we present our conclusions.

## II. BACKGROUND MODELS

In this section we briefly review the different models that, at the background level, lead to distinct future cosmological abrupt events: (i) Big Rip (BR), (ii) Little Rip (LR) and (iii) Little Sibling of the Big rip (LSBR). We will consider a homogeneous and isotropic Universe described by the Friedmann-Lemaître-Robertson-Walker (FLRW) metric:

$$ds^2 = -dt^2 + a^2(t) \left[ \frac{dr^2}{1 - kr^2} + r^2 d\theta^2 + r^2 \sin^2 \theta d\varphi^2 \right], \quad (2.1)$$

where  $a(t)$  is the scale factor and  $k = -1, 0, 1$  for open, flat and closed spatial geometry, respectively. We will focus on the spatially flat case ( $k = 0$ ), for which the Friedmann and Raychaudhuri equations read

$$H^2 = \frac{8\pi G}{3}\rho, \quad (2.2)$$

$$\dot{H} = -4\pi G(\rho + p). \quad (2.3)$$

Here,  $H$  is the Hubble parameter, a dot represents a derivative with respect to the cosmic time,  $t$ ,  $G$  is the cosmological constant and  $\rho$  and  $p$  are the total energy density and pressure of all the matter content of the Universe. In this work, we will consider the Universe to be filled by radiation, dust (cold dark matter and baryons), and DE. As such, we can decompose  $\rho$  and  $p$  as

$$\rho = \rho_r + \rho_m + \rho_d \quad \text{and} \quad p = p_r + p_m + p_d, \quad (2.4)$$

where  $\rho_r$ ,  $\rho_m$ , and  $\rho_d$  correspond to the energy density of radiation, matter (cold dark matter and baryonic) and DE. Similarly,  $p_r$ ,  $p_m$ , and  $p_d$  are the pressure of radiation ( $p_r = 1/3\rho_r$ ), matter ( $p_m = 0$ ), and DE ( $p_d = w_d\rho_d$ ). We will not take into account interactions between the individual matter components. Consequently, each fluid  $A = r, m, d$  verifies the usual conservation equation:

$$\dot{\rho}_A + 3H(\rho_A + p_A) = 0. \quad (2.5)$$

For latter convenience, we define the fractional energy density of the individual matter components as

$$\Omega_r = \frac{\rho_r}{\rho}, \quad \Omega_m = \frac{\rho_m}{\rho}, \quad \Omega_d = \frac{\rho_d}{\rho}, \quad (2.6)$$

and the individual parameters of EoS

$$w_r = \frac{p_r}{\rho_r} = \frac{1}{3}, \quad w_m = \frac{p_m}{\rho_m} = 0, \quad w_d = \frac{p_d}{\rho_d}. \quad (2.7)$$

The DE parameter of EoS,  $w_d$ , will be fixed later for each individual model. From (2.4) and (2.6) we can obtain the total parameter of EoS,  $w$ , from the individual  $w_A$  as:

$$w \equiv \frac{p}{\rho} = \Omega_r w_r + \Omega_m w_m + \Omega_d w_d. \quad (2.8)$$

In the following subsections, we present the three models which will be studied in this work. From this point onward a 0-subscript denotes the present value of a given quantity and we set  $a_0 = 1$ .

### A. BR singularity: model (i)

A BR singularity [17–24] can be induced by a perfect fluid whose EoS is constant and smaller than  $-1$ .

$$p_d = w_d \rho_d. \quad (2.9)$$

Therefore, using the conservation equation (2.5), the energy density evolves with the scale factor as

$$\rho_d(a) = \rho_{d0} a^{-3(1+w_d)}. \quad (2.10)$$

Finally, the asymptotic evolution of the scale factor is

$$a(t) \sim \left[ 1 + \frac{3}{2} (1 + w_d) H_0 \sqrt{\Omega_{d0}} (t - t_0) \right]^{\frac{2}{3(1+w_d)}}. \quad (2.11)$$

In this kind of future singularity, the scale factor, the Hubble parameter and its cosmic time derivatives blow up at a finite cosmic time. For the rest of the work, for the BR model we fix the free parameters of the models to the best fit in accordance with the Planck data for wCDM model [51]:  $w_d = -1.019$ ,  $\Omega_{m0} = 0.306$  and  $H_0 = 68.1 \text{ Km Mpc}^{-1}\text{s}^{-1}$  (please, cf. page 687 of [51]).

### B. LR abrupt event: model (ii)

The case of a LR [25–32] can be caused by a perfect fluid whose EoS fulfills [27, 29]

$$p_d = - \left( \rho_d + B \rho_d^{\frac{1}{2}} \right), \quad (2.12)$$

where the constant  $B$  is positive and has dimensions of inverse length square. Applying the conservation equation (2.5), the energy density in terms of the scale factor reads

$$\rho_d(a) = \rho_{d0} \left[ \frac{3}{2} \frac{B}{\sqrt{\rho_{d0}}} \ln \left( \frac{a}{a_0} \right) + 1 \right]^2. \quad (2.13)$$

Finally, the asymptotic future evolution of the scale factor can be written as [31]

$$a(t) \sim \exp \left( \frac{2}{3} \sqrt{\frac{\Omega_{d0}}{\Omega_*}} \left\{ \exp \left[ \frac{3}{2} \sqrt{\Omega_*} H_0 (t - t_0) - 1 \right] \right\} \right), \quad (2.14)$$

where  $\Omega_* \equiv 8\pi G B^2 / (3H_0^2)$ . In this kind of abrupt event, the scale factor, the Hubble parameter and its cosmic time derivatives blow up at an infinite cosmic time. To fix the values of the parameters of the model we choose the best fit found in [31], where the authors used the data of [52] to constrain the LR model observationally from a background point of view with respect to its evolution. The results obtained in [31] were  $\Omega_{m0} = 0.274$ ,  $H_0 = 70.1 \text{ Km Mpc}^{-1}\text{s}^{-1}$  and  $\Omega_* = 7.7637 \cdot 10^{-4}$ , and these are the values that we will use in this work.

### C. LSBR abrupt event: model (iii)

The LSBR can be induced by a perfect fluid whose EoS deviates from that of a cosmological constant as [33]

$$p_d = - \left( \rho_d + \frac{A}{3} \right), \quad (2.15)$$

where  $A$  is a positive constant and whose dimensions are length to the fourth power. Making use of the conservation equation (2.5), the energy density on this case reads

$$\rho_d(a) = \rho_{d0} + A \ln \left( \frac{a}{a_0} \right), \quad (2.16)$$

where  $\rho_{d0}$  plays the role of a cosmological constant. Finally, the future asymptotic growth of the scale factor with respect to the cosmic time can be written as [33]

$$a(t) \sim \exp \left( \frac{1}{\alpha} \left\{ \left[ \frac{\alpha}{2} \sqrt{\Omega_{d0}} H_0 (t - t_0) + 1 \right]^2 - 1 \right\} \right), \quad (2.17)$$

where we have introduced the dimensionless constant  $\alpha \equiv A/\rho_{d0}$ . In this type of abrupt event, the scale factor and the Hubble parameter blow up at infinite cosmic time. However, the cosmic time derivative of the Hubble parameter remains constant. For practical purposes, we will choose the numerical values taken in [33]:  $A = 10^{-3} (3H_0^2/8\pi G)$ . For  $\Omega_{m0}$  and  $H_0$ , we choose the same values used in the model (i) according to the Planck results [4, 51], i.e.  $\Omega_{m0} = 0.306$  being  $H_0 = 68.1 \text{ Km Mpc}^{-1}\text{s}^{-1}$ .

### III. PERTURBED EQUATIONS

In this section, we review the theory of linear perturbations for multi-fluid components. We choose the Newtonian gauge and work with the corresponding gauge invariant perturbation quantities. For a FLRW Universe, the perturbed line element is [53, 54]

$$ds^2 = a^2 [ - (1 + 2\Phi) d\eta^2 + (1 - 2\Psi) \delta_{ij} dx^i dx^j ], \quad (3.1)$$

where  $\eta$  is the comoving time,  $d\eta = (1/a)dt$ , the latin index denote purely spatial coordinates, and  $\Psi(\eta, x^i)$  and  $\Phi(\eta, x^i)$  are the gauge invariant Bardeen potentials [55]. The transformation rule  $\{\dot{\cdot}\} = (1/a)\{\cdot\}'$ , where a prime represents a derivative with respect to the conformal time, allows us to write  $H$  and  $\dot{H}$  in terms of the conformal Hubble parameter,  $\mathcal{H} \equiv a'/a$ , and its derivative,  $\mathcal{H}'$ , as

$$H = \frac{1}{a} \mathcal{H}, \quad \dot{H} = \frac{1}{a^2} (\mathcal{H}' - \mathcal{H}^2). \quad (3.2)$$

Drawing from the line element (3.1), the inverse of the metric tensor can be obtained applying a Taylor expansion up to first order. Once we define the Christoffel symbols, we can compute the perturbation of the Ricci tensor,  $\delta R_{\mu\nu}$ , and of the curvature scalar,  $\delta R$ , in order to obtain the perturbed Einstein tensor  $\delta G_{\mu\nu} \equiv \delta R_{\mu\nu} - \frac{1}{2}\delta^\mu_\nu \delta R$ . In addition, the perturbed Einstein equations read

$$\delta G^\mu_\nu = 8\pi G \delta T^\mu_\nu, \quad (3.3)$$

where  $\delta T^\mu_\nu$  is the linear perturbation of the total energy momentum tensor. The individual components of Eq. (3.3) can be written as [53, 54]

$$\begin{aligned} 3\mathcal{H}(\Psi' + \Phi\mathcal{H}) - \nabla^2 \Psi &= 4\pi G a^2 \delta T^0_0, \\ -(\Psi' + \mathcal{H}\Phi)_{,i} &= 4\pi G a^2 \delta T^0_i, \\ \Psi'' + 2\mathcal{H}(\Phi' + 2\Psi') + 2\Phi(2\mathcal{H}' + \mathcal{H}^2) \Phi + \frac{2}{3}\nabla^2(\Phi - \Psi) &= \frac{4\pi G}{3} a^2 \delta T^i_{,i}, \\ (\Phi - \Psi)_{,ij} &= 8\pi G a^2 \delta T^i_j, \quad (i \neq j). \end{aligned} \quad (3.4)$$

The  $\delta T^\mu_\nu$  on the right hand side of (3.3) is the sum of the perturbations of the energy momentum tensor of radiation,  $\delta T^{\mu}_{r\nu}$ , non-relativistic matter (cold dark matter and baryons),  $\delta T^{\mu}_{m\nu}$ , and DE,  $\delta T^{\mu}_{d\nu}$ . For each fluid, we can write the individual components of  $\delta T^{\mu}_{A\nu}$  ( $A = r, m, d$ ) as

$$\begin{aligned} \delta T^0_{A0} &= -\delta\rho_A, \\ \delta T^i_{A0} &= -(p + \rho) \partial^i v_A, \\ \delta T^0_{Ai} &= (p + \rho) \partial_i v_A, \\ \delta T^i_{Aj} &= \delta p_A \delta^i_j + \Pi^i_{Aj}, \end{aligned} \quad (3.5)$$

where  $\delta\rho_A$ ,  $\delta p_A$ ,  $v_A$ , and  $\Pi_{A,j}^i$  are, respectively, the perturbation of the energy density, the perturbation of the pressure, the peculiar velocity potential and the anisotropic stress tensor of the fluid  $A$ . In this work we consider that none of the fluids considered introduce anisotropies at the linear level of scalar perturbations, therefore, from this point onward we will set  $\Pi_{A,j}^i = 0$ . From Eq. (3.4), we find that this implies the equality of the metric potentials  $\Psi = \Phi$ . Replacing this equivalence and Eqs. (3.5) in the first three equations of (3.4), we obtain [53, 54]

$$\begin{aligned} 3\mathcal{H}(\mathcal{H}\Psi + \Psi') - \nabla^2\Psi &= -4\pi Ga^2\delta\rho, \\ \nabla^2(\mathcal{H}\Psi + \Psi') &= -4\pi Ga^2(\rho + p)\nabla^2v, \\ \Psi'' + 3\mathcal{H}\Psi' + \Psi(2\mathcal{H}' + \mathcal{H}^2) &= 4\pi Ga^2\delta p, \end{aligned} \quad (3.6)$$

where we have introduced the total energy density perturbation,  $\delta\rho$ , total pressure perturbation,  $\delta p$ , and total velocity potential,  $v$ . These can be written in terms of the individual fluid variables in Eqs. (3.5) through the relations

$$\delta\rho = \sum_A \delta\rho_A, \quad \delta p = \sum_A \delta p_A, \quad v = \sum_A \frac{1+w_A}{1+w} v_A. \quad (3.7)$$

Following [56, 57], we decompose the pressure perturbation as<sup>1</sup>

$$\delta p_A = c_{sA}^2 \delta\rho_A - 3\mathcal{H}(1+w_A)(c_{sA}^2 - c_{aA}^2)\rho_A v_A, \quad (3.8)$$

where

$$c_{sA}^2 = \left. \frac{\delta p_A}{\delta\rho_A} \right|_{\text{r.f.}}, \quad c_{aA}^2 = \frac{p'_A}{\rho'_A}, \quad (3.9)$$

are, respectively, the effective squared speed of sound defined in the rest frame (r.f.) of the fluid and the adiabatic speed of sound. In the following analysis, we will replace the energy density perturbation  $\delta\rho_A$  by the fractional energy density perturbation  $\delta_A = \delta\rho_A/\rho_A$ . The total perturbation  $\delta$  can be obtained from Eq. (3.7) and reads

$$\delta = \sum_A \frac{\rho_A}{\rho} \delta_A = \sum_A \Omega_A \delta_A. \quad (3.10)$$

The perturbed conservation equations of the energy-momentum tensor for each fluid read:

$$\nabla_\mu \delta T_{A\nu}^\mu + \delta\Gamma_{\mu\alpha}^\mu T_{A\nu}^\alpha - \delta\Gamma_{\mu\nu}^\alpha T_{A\alpha}^\mu = 0, \quad (3.11)$$

where  $\delta\Gamma_{\mu\nu}^\alpha$  is the perturbation of the Christoffel symbol and  $T_{A\nu}^\mu$  is the background value of the energy momentum tensor. Using Eqs. (3.5), (3.8), (3.9), and (3.11), we can compute the temporal and spatial components of Eq. (3.11) and obtain the evolution equations for the fractional energy density perturbation  $\delta_A$  and the velocity potential  $v_A$

$$\begin{aligned} \delta'_A &= 3\mathcal{H}(w_A - c_{sA}^2)\delta_A + (1+w_A)[9\mathcal{H}^2(c_{sA}^2 - c_{aA}^2) - \nabla^2]v_A + 3(1+w_A)\Psi', \\ v'_A &= (3c_{sA}^2 - 1)\mathcal{H}v_A - \frac{c_{sA}^2}{1+w_A}\delta_A - \Psi. \end{aligned} \quad (3.12)$$

In summary, from the perturbed Einstein equation, we obtain Eqs. (3.6) which relate the metric perturbations to the total perturbed matter quantities. On the other hand, from the perturbed conservation equations we obtain Eqs. (3.12) which dictate the dynamics for the individual energy density and velocity perturbations.

In order to study the evolution of the linear perturbations, we have conveniently applied a Fourier transformation, where we decompose a given function  $\psi(\eta, \mathbf{x})$  into its Fourier components  $\psi_k(\eta)$  as

$$\psi(\eta, \mathbf{x}) = \frac{1}{(2\pi)^{3/2}} \int e^{-i\mathbf{k}\cdot\mathbf{x}} \psi_k(\eta) d^3\mathbf{k}. \quad (3.13)$$

Therefore, for practical purposes, we make the substitution  $\nabla^2 \rightarrow -k^2$  in all the evolution equations. On the other hand, we will apply the following change of variable:

$$x \equiv \ln(a), \quad \{\} = \{\}_x \mathcal{H}, \quad \{\}'' = \{\}_{xx} \mathcal{H}^2 + \{\}_x \mathcal{H}', \quad (3.14)$$

---

<sup>1</sup> The re-derive this expression is presented in the Appendix A.

where the subscript  $x$  denotes a derivative with respect to  $x$ . By applying the Fourier decomposition (3.13) and the transformation (3.14) to the sets of equations (3.6) and (3.12), we obtain the evolution equations for each mode of the energy density and velocity perturbations of radiation, dust and dark energy

$$\begin{aligned}
(\delta_r)_x &= \frac{4}{3} \left( \frac{k^2}{\mathcal{H}} v_r + 3\Psi_x \right), \\
(v_r)_x &= -\frac{1}{\mathcal{H}} \left( \frac{1}{4} \delta_r + \Psi \right), \\
(\delta_m)_x &= \left( \frac{k^2}{\mathcal{H}} v_m + 3\Psi_x \right), \\
(v_m)_x &= - \left( v_m + \frac{\Psi}{\mathcal{H}} \right), \\
(\delta_d)_x &= (1 + w_d) \left\{ \left[ \frac{k^2}{\mathcal{H}} + 9\mathcal{H} (1 - c_{ad}^2) \right] v_d + 3\Psi_x \right\} + 3(w_d - 1) \delta_d, \\
(v_d)_x &= -\frac{1}{\mathcal{H}} \left( \frac{1}{1 + w_d} \delta_d + \Psi \right) + 2v_d.
\end{aligned} \tag{3.15}$$

and for the metric potential

$$\begin{aligned}
\Psi_x + \Psi \left( 1 + \frac{k^2}{3\mathcal{H}^2} \right) &= -\frac{1}{2} \delta, \\
\Psi_x + \Psi &= -\frac{3}{2} \mathcal{H} v (1 + w), \\
\Psi_{xx} + \left[ 3 - \frac{1}{2} (1 + 3w) \right] \Psi_x - 3w\Psi &= \frac{3}{2} \frac{\delta p}{\rho}.
\end{aligned} \tag{3.16}$$

### A. The speed of sound of DE

So far, in this work we have described all the individual matter components as perfect fluids with a barotropic equations of state  $p_A(\rho_A)$ . Since a barotropic fluid is adiabatic, for such fluid the effective and adiabatic squared speeds of sound are the same (cf. Eq. (3.9)). While for radiation and matter such a representation works well, for fluids with negative EoS, in particular for fluids playing the role of DE, there might be some problems if the squared speed of sound becomes negative, which would lead to instabilities at the perturbative level. As a matter of extra-clarification we discuss in the Appendix B how instabilities at the linear level in perturbations arise in fluids with a negative adiabatic squared speed of sound. It is therefore necessary to take into account additional considerations for the DE fluid. To avoid this problem we employ the same strategy used in [56, 57] and map the DE fluid to a phantom scalar field<sup>2</sup>,  $\varphi$ , whose energy density and pressure perturbations can be written as

$$\delta\rho_\varphi = -\dot{\varphi}(\delta\dot{\varphi} + \dot{\varphi}\Psi) + \frac{\delta V}{\partial\varphi}\delta\varphi, \tag{3.17}$$

$$\delta p_\varphi = -\dot{\varphi}(\delta\dot{\varphi} + \dot{\varphi}\Psi) - \frac{\delta V}{\partial\varphi}\delta\varphi. \tag{3.18}$$

In the rest frame of the phantom scalar field, which is defined by the surfaces with constant value of  $\varphi$ , i.e.  $\delta\varphi = 0$  [56, 57], we find that  $\delta p_\varphi/\delta\rho_\varphi = 1$  and therefore the effective squared speed of sound of DE, as defined in (3.9), is equal to unity. For each DE model that we consider, we will therefore set  $c_{sd}^2 = 1$  in Eqs. (3.15), while  $c_{ad}^2$  is given by Eq. (3.9). As we will show below, this mapping of the DE fluid to a phantom scalar field removes any instabilities in the energy density of the scalar perturbations of DE overcoming through this phenomenological approach the classical perturbative pathologies associated to some phantom DE models.

---

<sup>2</sup> In Refs. [56, 57] a canonical scalar field is considered when mapping the DE perturbations. However, in this work we are considering phantom DE models, therefore with equations of state such that  $w_d < -1$ . Since a canonical scalar field with positive potentials cannot achieve the values  $w_d < -1$ , here we consider that our DE fluid corresponds to a phantom scalar field [18].

## B. Initial conditions

Once the system of equations of the perturbed quantities is defined, we need to impose proper initial conditions in order to compute the cosmological evolution of the perturbations (cf. for example [58, 59] for a detailed discussion on the initial conditions on DE models). For this goal, we will take into account the following considerations. First, we assume that at an initial moment,  $z \sim 10^6$  (which roughly corresponds to  $x_* \sim -14$ ), the Universe is completely dominated by radiation, so that all relevant quantities of the total matter fluid are those of a perfect fluid with  $p = \rho/3$ . Secondly, we note that at such moment the wave-length of all the relevant modes is small when compared with the comoving Hubble parameter ( $k \ll \mathcal{H}$ ), i.e. they are outside the horizon. With these two approximations, we can combine the first and third equations of (3.16) and obtain a closed evolution equation for the metric potential in the asymptotic past [11]

$$\Psi_{xx} + 3\Psi_x \approx 0. \quad (3.19)$$

The dominant solution of this equation is a constant solution  $\Psi = \Psi(x_*)$ . Applying this result to the set of equations (3.16), we find that initially

$$\begin{aligned} \Psi(x_*) &\approx -\frac{1}{2}\delta(x_*) , \\ \Psi(x_*) &\approx -2\mathcal{H}(x_*)v(x_*) . \end{aligned} \quad (3.20)$$

Assuming initial adiabatic conditions, we can relate the initial values of the individual fluid perturbed variables to the total perturbation in Eq. (3.20) through [11, 58, 59]

$$\frac{\delta_r}{1+w_r} = \frac{\delta_m}{1+w_m} = \frac{\delta_d}{1+w_d} = \frac{\delta}{1+w}. \quad (3.21)$$

This allows us to write the initial values of  $\delta_A$  in terms of  $\delta(x_*)$  as

$$\frac{3}{4}\delta_r(x_*) = \delta_m(x_*) = \frac{\delta_d(x_*)}{1+w_d(x_*)} \approx \frac{3}{4}\delta(x_*) , \quad (3.22)$$

By imposing the adiabatic condition (3.21) on the comoving gauge, we obtain

$$\frac{\delta_A(x_*) - 3\mathcal{H}(x_*)[1+w_A(x_*)]v_A(x_*)}{1+w_A(x_*)} = \frac{\delta_B(x_*) - 3\mathcal{H}(x_*)[1+w_B(x_*)]v_B(x_*)}{1+w_B(x_*)} , \quad (3.23)$$

which then leads to the initial values of the peculiar velocities  $v_A$ :

$$v_r(x_*) = v_m(x_*) = v_d(x_*) \approx \frac{\delta(x_*)}{4\mathcal{H}(x_*)} . \quad (3.24)$$

We note that the conditions (3.22) and (3.24) coincide with the ones presented in [58] in the absence of neutrinos. Making use of the linearity of Eqs. (3.15) and (3.16), we can first compute the evolution of the perturbation quantities using the initial conditions (3.20), (3.22) and (3.24) for  $\Psi(x_*) = 1$  (which implies  $\delta(x_*) = -2$ ) and then multiply all the solutions obtained by the physical value of  $\delta_{\text{phys}}(k)$ , which we will take from the Planck observational fit to single field inflation and given as [4]

$$\delta_{\text{phys}}(k) = \frac{8\pi}{3}\sqrt{2A_s}\left(\frac{k}{k_*}\right)^{\frac{n_s-1}{2}}k^{-\frac{3}{2}} . \quad (3.25)$$

Here,  $A_s$  and  $n_s$  are defined as the amplitude and spectral index of the primordial inflationary power spectrum corresponding to a previously selected pivot scale  $k_*$ . In this work, we will use the values  $k_* = 0.05 \text{ Mpc}^{-1}$ ,  $A_s = 2.143 \cdot 10^{-9}$ , and  $n_s = 0.9681$  in accordance with Planck observational data<sup>3</sup> [4].

---

<sup>3</sup> Strictly speaking, for the model (ii) we should have taken the data of WMAP7 [52], since that was the data used in [31] to constrain the parameters of the model (ii). This was precisely what we have done. However, it turns out that our results for the model (ii) do not change significantly by changing  $A_s$ ,  $n_s$  and the pivot scale to those of WMAP7.

### C. Matter power spectrum and the growth rate

The matter power spectrum describes how galaxies are distributed along the Universe and provides us with a method to compare the theoretical predictions with the observational data. In this work, we will compute the linear matter power spectrum for each model studied in Sec. II and we will try to detect deviations from the predictions of  $\Lambda$ CDM. The whole framework presented in the previous sections provide us the necessary tools to obtain the aimed results. Notice, however, that the correct definition of the matter power spectrum uses the fractional energy density perturbation in the comoving gauge [60, 61], while the analysis carried out in this work has been done in the Newtonian gauge. Using the variables employed in the previous sections, we can resolve this gauge difference by expressing the matter power spectrum as

$$P_{\hat{\delta}_m} = \left| \delta_m^{(com)} \right|^2 = |\delta_m - 3\mathcal{H}v_m|^2. \quad (3.26)$$

Another method we will use to constrain the models presented in Section II is based in computing the growth rate of the matter perturbations for the different models. By definition, the growth rate of the matter perturbations is given by the formula [46]

$$f \equiv \frac{d(\ln \delta_m)}{d(\ln a)}. \quad (3.27)$$

For DM-DE models that closely mimic  $\Lambda$ CDM, it was found that the growth rate at late-time can be approximated reasonably well by the formula [62–64]

$$f \simeq \Omega_m^\gamma, \quad (3.28)$$

where  $\gamma \simeq 0.55$  for  $\Lambda$ CDM. The next leading order of (3.28) can be found in [51].

In this work, instead of using any approximated parametrisation, we opt to calculate the evolution of the growth rate  $f$  for each DE model using the full Eqs. (3.15)–(3.16) and compare the results with observations. We note, however, that in most cases, the observational data refers not to the growth rate  $f$  directly, but to the combination  $f\sigma_8$ , where  $\sigma_8$  is the root mean square mass fluctuation amplitude in spheres of size  $8h^{-1}\text{Mpc}$  which is used to normalise the matter power spectrum. This combination has the advantage that it avoids the degeneracy in the parameter space regarding  $\sigma_8$  and the linear bias,  $b$ , between the perturbations of dark matter and density of galaxies [65]. We calculate the temporal evolution of  $\sigma_8$  by the formula<sup>4</sup> [66]

$$\sigma_8(z, k_{\sigma_8}) = \sigma_8(0, k_{\sigma_8}) \frac{\delta_m(z, k_{\sigma_8})}{\delta_m(0, k_{\sigma_8})}. \quad (3.29)$$

where  $k_{\sigma_8} = 0.125 \text{ hMpc}^{-1}$  is the wave-length of the mode corresponding to distances of  $8h^{-1}\text{Mpc}$ .

For each of the DE models considered in this work, we will calculate the evolution of  $f\sigma_8$  using the numerical solutions of Eqs. (3.15)–(3.16) and the relations (3.27) and (3.29). For the models (i) and (iii) we use  $\sigma_8(0, k_{\sigma_8}) = 0.820$  [51] as the present day value of  $\sigma_8$ , while for the model (ii) we use the value  $\sigma_8(0, k_{\sigma_8}) = 0.809$  [52]. We compare the results obtained with the available observational data [65, 67–81] to check whether the predictions of the models are within the observational constraints. Since at the background level these models are very similar to  $\Lambda$ CDM till the present time, we expect that the deviations from  $\Lambda$ CDM in the evolution of the growth rate to be small.

## IV. RESULTS

In this section, we present and discuss the results obtained for the evolution of the cosmological perturbations in the three models discussed in Sec II that contain distinct future cosmological abrupt events:

- i) a Big Rip singularity (Sec. II A),
- ii) a Little Rip event (Sec. II B)
- iii) a Little Sibling of the Big Rip event (Sec. II C).

---

<sup>4</sup> We thank V. Salzano for clarifying this point to us.

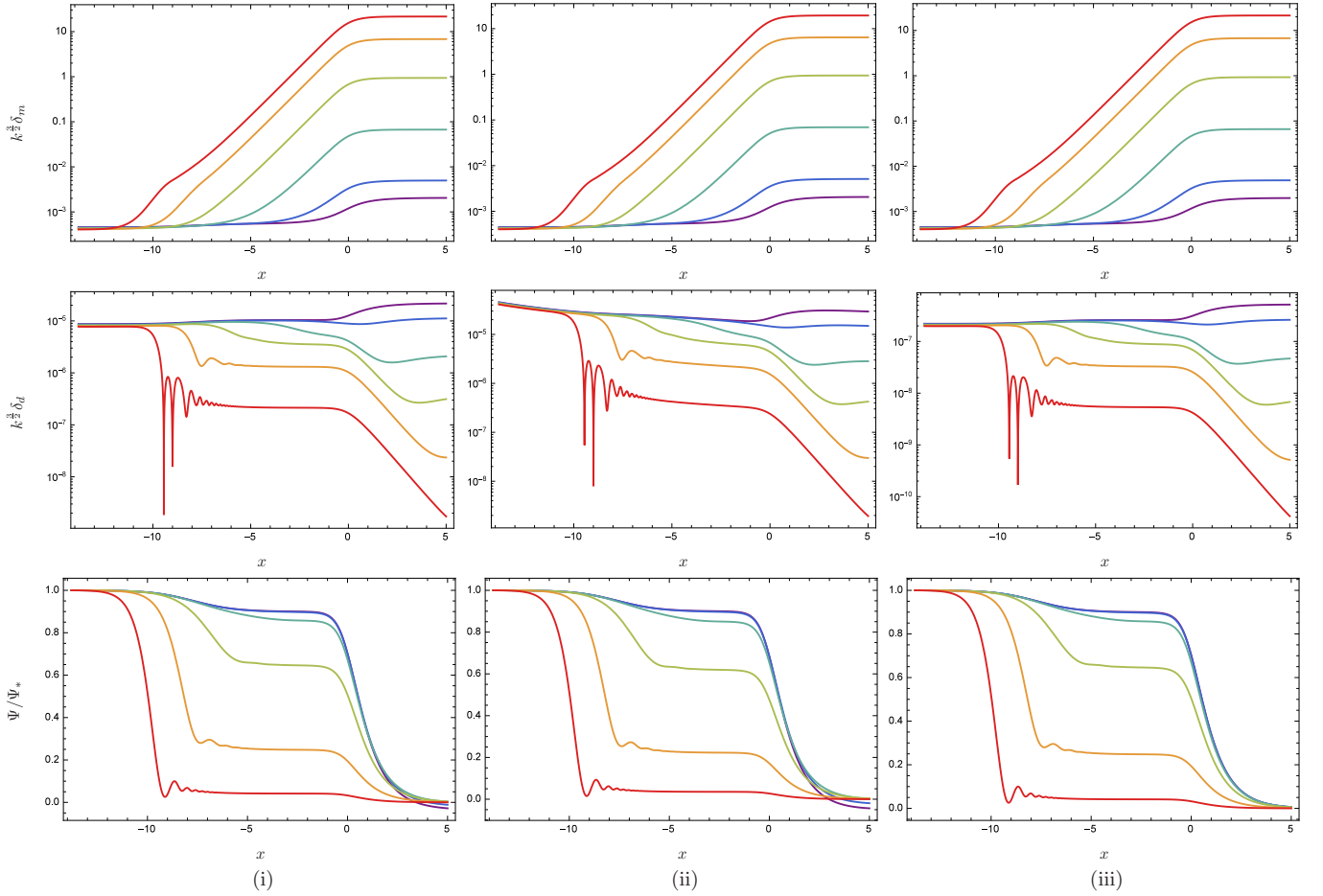


FIG. 1. In this figure the first column (i) shows the results of the BR model, the second column (ii) shows the results of the LR model, and the third column (iii) shows the results of the LSBR model. The first row corresponds to the DM perturbations while the second row corresponds to the DE perturbations. In both cases the initial value of the perturbations is given by Eqs. (3.22) and (3.25). The third row corresponds to the perturbation of the gravitational potential normalised to the initial value  $\Psi_*$ . Each colour represent a mode where the values of the corresponding wave-number are:  $k = 3.33 \times 10^{-4}h \text{ Mpc}^{-1}$  (purple),  $k = 7.93 \times 10^{-4}h \text{ Mpc}^{-1}$  (dark blue),  $k = 3.50 \times 10^{-3}h \text{ Mpc}^{-1}$  (light blue),  $k = 1.54 \times 10^{-2}h \text{ Mpc}^{-1}$  (green),  $k = 6.80 \times 10^{-2}h \text{ Mpc}^{-1}$  (orange),  $k = 0.30h \text{ Mpc}^{-1}$  (red). All perturbations are represented versus  $x = \log(a/a_0)$  which varies from values well inside the radiation era ( $x = -13.81$ ) till the far future ( $x = 5$ ). The value  $x = 0$  corresponds to the present time.

For each of these models, the evolution of the matter perturbations  $\delta_m$ ,  $v_m$ ,  $\delta_r$ ,  $v_r$ ,  $\delta_d$ , and  $v_d$  was obtained by numerically integrating the set of Eqs. (3.15) after substituting  $\Psi$  and  $\Psi_x$  given in (3.16). After carrying this numeric integration, the gravitational potential  $\Psi$  and its derivative  $\Psi_x$  can be obtained from the first two equations in (3.16). The integration was performed since an initial moment deep inside the radiation epoch ( $z \sim 10^6$ ), when all the relevant modes are outside the horizon, and till a point in the distant future ( $z \sim -0.99$ ). At the initial moment, the values of the variables were fixed according to Eqs. (3.22), (3.24) and (3.25). In addition, for each model this integration was repeated for 40 different modes with wave-numbers ranging from  $k_{\min} \sim 3.3 \times 10^{-4}h \text{ Mpc}^{-1}$ , which corresponds to the mode that is exiting the Hubble horizon at the present time, to a  $k_{\max} \sim 3.0 \times 10^{-1}h \text{ Mpc}^{-1}$ . Notice that for  $k \gtrsim k_{\max}$  the validity of the linear perturbation theory breaks down as non-linear effects start to become dominant in the evolution of the perturbations. In fact,  $k_{\max}$  should be at most  $2.0 \times 10^{-1}h \text{ Mpc}^{-1}$ . On the plots we included the the higher value  $k_{\max} \sim 3.0 \times 10^{-1}h \text{ Mpc}^{-1}$  to amplify visually the effect and evolution on the largest modes.

In Fig. 1, we illustrate the evolution of the cosmological perturbations, since the initial moment and till a point in the future evolution of the Universe. The first and second rows present, respectively, the evolution for the fractional energy densities of DM,  $\delta_m$ , and DE,  $\delta_d$ , while the third row presents the evolution of the gravitational potential,  $\Psi$ , which has been normalised with respect to its initial value,  $\Psi_*$ . For each of these quantities, we plot the results for 6 different wave-numbers:  $k = 3.33 \times 10^{-4}h \text{ Mpc}^{-1}$  (purple),  $k = 7.93 \times 10^{-4}h \text{ Mpc}^{-1}$  (dark blue),  $k = 3.50 \times 10^{-3}h \text{ Mpc}^{-1}$  (light blue),  $k = 1.54 \times 10^{-2}h \text{ Mpc}^{-1}$  (green),  $k = 6.80 \times 10^{-2}h \text{ Mpc}^{-1}$  (orange), and  $k = 0.30h \text{ Mpc}^{-1}$  (red). In

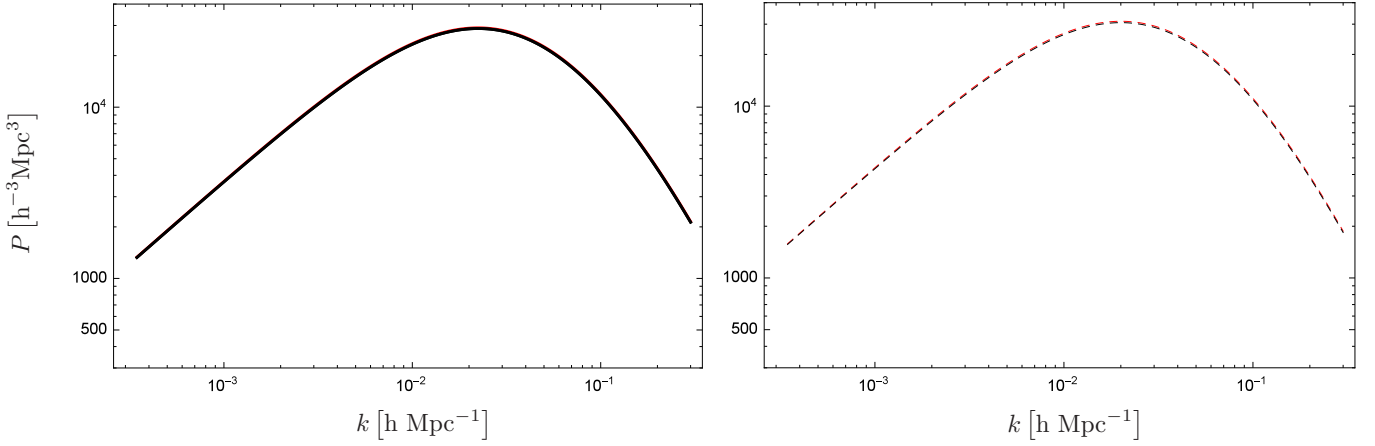


FIG. 2. This figure shows the matter power spectrum at redshift  $z = 0$ . On the left hand side panel, we plot the matter power spectrum of the models (i) and (iii) together with the matter power spectrum given by  $\Lambda\text{CDM}$  using the parameters provided by Planck [4, 51]. There is no observable difference between these three models, consequently, they look as a single curve. On the right hand side panel, we plot the matter power spectrum corresponding to the model (ii) (dashed red), together with the  $\Lambda\text{CDM}$  model (dashed black) in order to distinguish potential deviations between the two models. Here, the numerical values are chosen accordingly with the fit obtained in [31] using the WMAP7 data [52].

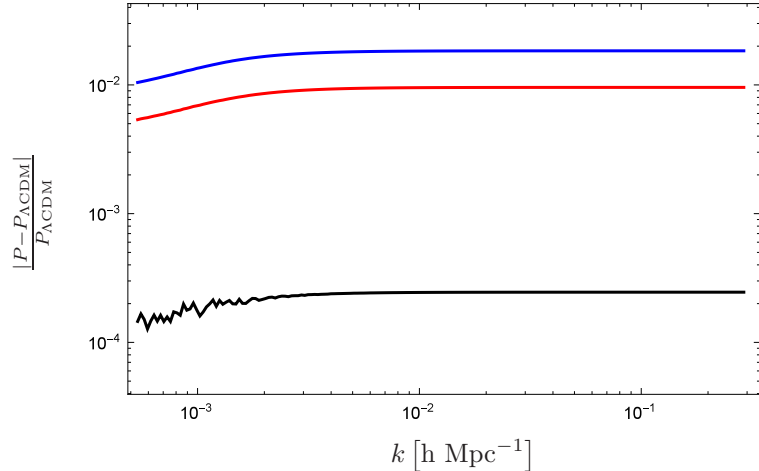


FIG. 3. This figure shows the relative deviation of each model in comparison with the corresponding  $\Lambda\text{CDM}$  model. The red curve corresponds to the model (i), the blue curve corresponds to the model (ii) and the black curve corresponds to the model (iii). The model that induces a BR singularity shows the highest deviation while the model that induces a LSBR abrupt event presents the smallest deviation respect to the  $\Lambda\text{CDM}$  model. The information encoded on this figure has to be taken with care as we assumed an  $\Omega_m$  corresponding to the Planck data [4, 51] for the models (i) and (iii) and to WMAP7 data [52] for the model (ii). This choice for the model (ii) was motivated by the fact that the only available cosmological constraint for such model [31] was done using the WMAP7 data.

terms of evolution, we can distinguish three different behaviours, according to the range of the wave-numbers:

- large  $k$ :  $0.30 \text{ hMpc}^{-1}$  (red) and  $6.80 \times 10^{-2} \text{ hMpc}^{-1}$  (orange).
- medium  $k$ :  $1.54 \times 10^{-2} \text{ hMpc}^{-1}$  (green) and  $3.50 \times 10^{-3} \text{ hMpc}^{-1}$  (light blue).
- small  $k$ :  $7.93 \times 10^{-3} \text{ hMpc}^{-1}$  (dark blue) and  $3.33 \times 10^{-4} \text{ hMpc}^{-1}$  (purple).

In addition, the results for the three models studied are separated in individual columns, with the first column corresponding to the BR model, i.e. (i), the second column to the LR model, i.e. (ii), and the third to the LSBR model; i.e. (iii) (c.f. Sec II).

As can be seen on the first row of Fig. 1, the matter perturbations for the different models present an almost identical behaviour. During the initial radiation dominated epoch, each individual mode remains constant until it enters the

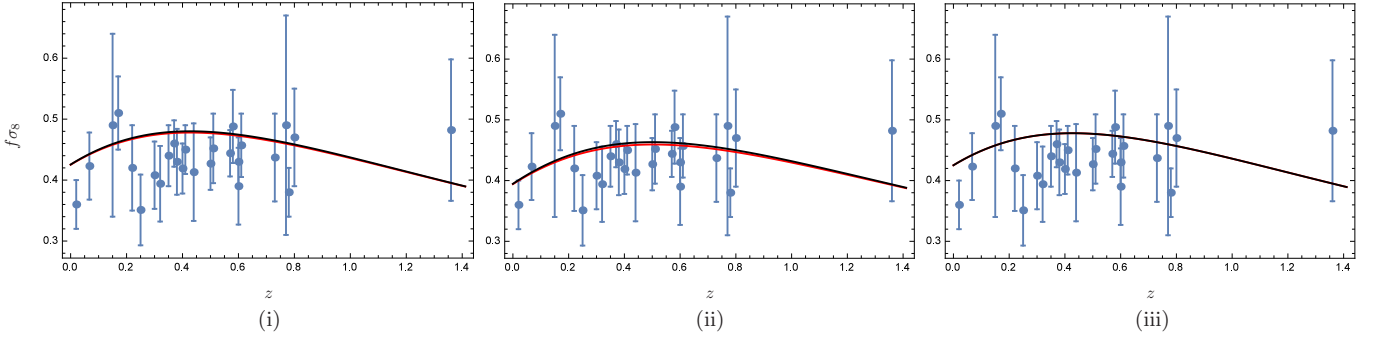


FIG. 4. This figure presents, in terms of the redshift, the evolution of  $f\sigma_8$  for each model (black curve) together with the corresponding  $\Lambda$ CDM model (red curve). The theoretical results obtained in this work are plotted against the observational values (blue dots with error bar) according with the data given in Table I. Our comments in Fig. 3 about the susceptibility of the results with the value of  $\Omega_m$  taken from different datasets applies equally here and can be extended to the plots in this figure.

Hubble horizon. After this point, the gravitational collapse leads to the growth of  $\delta_m$ , which becomes exponential in  $x$  during the matter era. Once the DE starts to become dominant, the growth of the matter perturbations slows down as  $\delta_m$  seems to converge to a constant value in the asymptotic future. Notice that since the modes with larger  $k$  enter the horizon at earlier time, they correspond to the curves with higher values of  $\delta_m$  in Fig. 1.

On the second row of Fig. 1, we present the evolution of the fractional energy density of DE for different wave-numbers. In contrast with the perturbations of DM, here we observe some small differences between the three models. First, we note that while in models (i) and (iii) all modes start with an almost constant behaviour, in model (ii) we can detect a slight decay of  $\delta_d$  during the radiation epoch, even when the modes are outside the horizon. Furthermore, from one model to the other, the amplitude of  $\delta_d$  for the same wave-number can vary more than two orders of magnitude. These differences can be explained by the great sensibility of the evolution equations (3.15) and the initial adiabatic conditions (3.21) to values of the EoS parameter  $w_d \sim -1$ . This sensibility amplifies the small differences in the behaviour of  $w_d$  for the three models, which is then propagated to both the initial value of  $\delta_d$  and its evolution during the early radiation epoch. At late time, we find that the differences in magnitude of the initial conditions of  $\delta_d$  in each model are maintained and can therefore serve as an imprint of the DE model.

Similarly to what happens with the DM perturbations, we can characterise the qualitative evolution of  $\delta_d$  in terms of the range of the wave-number of the mode:

- large  $k$ : These modes are the first to enter the horizon during the radiation epoch. After the horizon crossing their amplitude decays and we observe a damped oscillatory behaviour till the radiation-matter equality. At this point the modes stabilise and present a plateau that lasts until the end of the matter era. Once DE starts to dominate they start to decay rapidly once more.
- medium  $k$ : In this range, the modes present a behaviour of transition. While they enter the horizon only in the matter era, and therefore present no early oscillations, we still observe the existence of a plateau during the matter dominated era. The length of the plateau depends on the horizon crossing time - for the modes with smaller  $k$  the amplitude does not have time to stabilise before the DE dominated epoch. At this point, the amplitude starts to decay but, much like what happens for modes in the small  $k$  range, it stabilises once the accelerated expansion shrinks the Hubble radius and leads the modes to exit the horizon.
- small  $k$ : These modes are outside of the horizon for most of their evolution and therefore present little to no variation in amplitude till close to the present time, when they enter the horizon. At this point we observe a difference in behaviour, with the modes with smallest wave-numbers being amplified during the initial stages of the DE dominated epoch, while the largest modes in this range present a slight decay. Once the DE fluid completely dominates, however, the modes exit the horizon and their amplitude stabilises once more.

Despite all the differences in behaviour and amplitude between distinct models and modes, we always find that the amplitude of DE perturbations is extremely small when compared to DM. This validates the usual assumption of a DE smooth fluid.

On the third row of Fig. 1, we present the evolution of the gravitational potential  $\Psi$ . As can be seen, for all the ranges of  $k$  the perturbations start with a constant value at the radiation dominated epoch, during matter dominated era they reach a second plateau and finally vanish in the far future when DE gains importance. Nevertheless, we can identify some qualitative differences in the evolution of  $\Psi$ , depending on the range of  $k$ :

- large  $k$ : Initially, during the radiation epoch we observe a constant behaviour, these modes decay and oscillate once they enter the Hubble horizon. Then, during the matter dominated era the oscillations are suppressed and the perturbations reach a constant value till DE gains importance. At this point,  $\Psi$  starts to decay and vanishes asymptotically.
- medium  $k$ : The gravitational potential remains constant during the radiation dominated epoch, decays around the radiation-matter equality and reaches a second plateau in the matter dominated era. The decay observed in the transition between the two epochs is scale dependent and affects mostly the modes with higher wave-number. Finally, when dark energy takes over, the modes decay rapidly, vanishing in the far future.
- small  $k$ : As in the previous case, the modes corresponding to the smallest wave-numbers show a constant behaviour during the radiation dominated and the matter dominated epochs and a decay around the radiation-matter equality. Here, however, the decay is scale independent and for all the modes the amplitude of  $\Psi/\Psi_*$  during the matter era is 9/10 of its initial value, as follows from the theoretical prediction in the limit  $k \rightarrow 0$  [11]. Once DE begins to dominate, we observe a rapid decay of  $\Psi$ , with the gravitational potential vanishing in the future. Here, we mention the exceptional cases of the model (i) and (ii) for which the value of  $\Psi$  for the smaller modes does not appear to vanish. Instead, it evolves to negative values in the future, an effect which is particularly visible in the model (ii). This results indicates that gravity becomes repulsive which is in agreement with the rip of the cosmological structures.

In Fig. 2 we compare the theoretical matter power spectrum  $P_{\delta_m}$  obtained for each of the considered models with the one predicted by  $\Lambda$ CDM. As mention in Sec. II, the cosmological parameters for the models (i) and (iii) were adjusted with the recent Planck data [4, 51] while in the model (ii) the WMAP7 data [52] was used [31] (see the paragraph after Eq. (2.14)). As such, we present on the left panel of Fig. 2, the matter power spectra computed for the models (i) and (iii) and for  $\Lambda$ CDM with  $\Omega_{m0} = 0.306$  and  $H_0 = 68.1 \text{ Km Mpc}^{-1}\text{s}^{-1}$  [51], while on the right panel we present the matter power spectrum computed for the model (ii) and for  $\Lambda$ CDM with  $\Omega_{m0} = 0.274$  and  $H_0 = 70.1 \text{ Km Mpc}^{-1}\text{s}^{-1}$ . For all the cases, we find an almost perfect superposition of the results of the models (i), (ii) and (iii) with the ones of  $\Lambda$ CDM. This reflects the close resemblance in terms of evolution of all the models up to the present time and shows that observables like the matter power spectrum may not be able to distinguish dark energy models that do not differ significantly from  $\Lambda$ CDM till today.

In order to draw a comparison between the models, we compute the relative error with the corresponding  $\Lambda$ CDM model in each case. As can be seen in Fig. 3, for large values of the wave-number  $k$ , all models present a constant difference respect to the  $\Lambda$ CDM model while for small values of  $k$  the deviation is smaller. In all cases, the relative error is less than 0.02. The model (i) shows the largest deviation while the model (iii) is better adjusted to the  $\Lambda$ CDM model. Notice, that the model (iii) has not been observationally constrained and we took suitable values for the model parameters such that the model do not deviate too much from  $\Lambda$ CDM. We have fixed the value of the parameter  $A$  to be small enough to ensure a good approximation, as was done in Ref. [33]. For  $A = 0$ , we recover the  $\Lambda$ CDM model (See Sec II), i.e. the smaller is the value of  $A$ , the closer we are from the  $\Lambda$ CDM model.

Finally, in Fig. 4 we present the evolution of  $f\sigma_8$  of the three models (black curve) against several observational points in the range  $z \in (0, 1.4)$  (cf. Table I). For comparison, we represent as well the evolution of  $f\sigma_8$  for the corresponding  $\Lambda$ CDM model (red curve). Notice that, just like in the case of the matter power spectrum, the curve of the models (i), (ii) and (iii) are almost indistinguishable from the respective curve for  $\Lambda$ CDM. We find that all models are within the error bars for almost all of the points. Nevertheless, there seems to be some tension between the theoretical predictions and the observational data, in particular for the models (i) and (iii), as the  $f\sigma_8$  curves are systematically above most of the data points for redshifts up to  $z \sim 0.8$ . This higher tension between the theoretical predictions and the data in the models (i) and (iii) seems to come from the fact that for those models we used the Planck data which has a higher value of  $\Omega_{m0}$  than the WMAP7 data used for the model (ii). We note that the formation of structure is more intense, i.e.,  $f$  is larger, for higher values of  $\Omega_{m0}$  (cf. Eq. (3.28)). A more detailed discussion on this topic can be found in [82, 83].

In order to better understand which of these three models fits better the observational data, we compute for each of them the value of  $\chi^2$ , which can be written as

$$\chi^2 = \sum_i \frac{[f_{obs}(z_i) - f_{th}(z_i)]^2}{\sigma_i^2}. \quad (4.1)$$

Here,  $f_{obs}(z_i)$  and  $f_{th}(z_i)$  are, respectively, the observational and the theoretical growth rates at redshift  $z_i$ , while  $\sigma_i$  is the corresponding error for each measurement. The results obtained are:  $\chi^2_{(i)} = 27.63$  for the model (i),  $\chi^2_{(ii)} = 16.53$  for the model (ii), and  $\chi^2_{(iii)} = 26.30$  for the model (iii). We thus find that the model (ii) presents the smallest  $\chi^2$ , while the models (i) and (iii) have higher but similar values, with the model (iii) presenting the smallest  $\chi^2$  between

$z$	$f\sigma_8$	Survey	Ref.
0.02	$0.36 \pm 0.04$		[67]
0.067	$0.423 \pm 0.055$	6dF Galaxy Survey	[68]
0.15	$0.49 \pm 0.15$	SDSS DR7 MGS	[69]
0.17	$0.51 \pm 0.06$	2dF Galaxy Redshift Survey	[65, 70]
0.22	$0.42 \pm 0.07$	WiggleZ Dark Energy Survey	[71]
0.25	$0.351 \pm 0.058$	SDSS II LRG	[72]
0.3	$0.407 \pm 0.055$	SDSS I/II LRG + SDSS III BOSS CMASS	[74]
0.32	$0.394 \pm 0.062$	SDSS III BOSS DR12 LOWZ	[75]
0.35	$0.440 \pm 0.05$	SDSS DR5 LRG	[65, 76]
0.37	$0.460 \pm 0.038$	SDSS II LRG	[72]
0.38	$0.430 \pm 0.054$	SDSS III BOSS DR12	[73]
0.4	$0.419 \pm 0.041$	SDSS I/II LRG + SDSS III BOSS CMASS	[74]
0.41	$0.45 \pm 0.04$	WiggleZ Dark Energy Survey	[71]
0.44	$0.413 \pm 0.080$	WiggleZ Dark Energy Survey + Alcock-Paczynski distortion	[77]
0.5	$0.427 \pm 0.043$	SDSS I/II LRG + SDSS III BOSS CMASS	[74]
0.51	$0.452 \pm 0.057$	SDSS III BOSS DR12	[73]
0.57	$0.444 \pm 0.038$	SDSS III BOSS DR12 CMASS	[75]
0.59	$0.488 \pm 0.06$	SDSS III BOSS DR12 CMASS	[78]
0.60	$0.43 \pm 0.04$	WiggleZ Dark Energy Survey	[71]
0.6	$0.433 \pm 0.067$	SDSS I/II LRG + SDSS III BOSS CMASS	[74]
0.60	$0.390 \pm 0.063$	WiggleZ Dark Energy Survey + Alcock-Paczynski distortion	[77]
0.61	$0.457 \pm 0.052$	SDSS III BOSS DR12	[73]
0.73	$0.437 \pm 0.072$	WiggleZ Dark Energy Survey + Alcock-Paczynski distortion	[77]
0.77	$0.490 \pm 0.18$	VIMOS-VLT Deep Survey	[65, 79]
0.78	$0.38 \pm 0.04$	WiggleZ Dark Energy Survey	[71]
0.8	$0.470 \pm 0.08$	VIMOS Public Extragalactic Redshift Survey	[80]
1.36	$0.482 \pm 0.116$	FastSound	[81]

TABLE I. This table shows the available observational data points for  $f\sigma_8$  at different redshifts, which are plotted in Fig. 4. For each data point we present, in order, the value of the effective redshift, the value of  $f\sigma_8$  and respective error, the corresponding survey, and the reference from which the values were taken.

the two. This confirms the visual analysis of Fig. IV which suggests that the model (ii), is the one that better fits the observational data.

## V. CONCLUSIONS

In this work, we analyse the cosmological perturbations within the framework of GR, taking into full account the presence of DE at the perturbative level. The DE component is described by three different models, where each one of them behaves almost as  $\Lambda$ CDM model at present but induces a unique doomsday scenario in the future: model (i) leads to a BR; model (ii) leads to a LR; model (iii) leads to a LSBR. At late time, the parameter of EoS of DE for each of these models is very close to but slightly smaller than  $-1$ , thus corresponding to a phantom-like behaviour of DE. Despite the small variations of the parameter of the EoS for the three models, the asymptotic behaviour of the Universe is quite different from the one in  $\Lambda$ CDM, with the unavoidable rip of all the structure in the Universe no matter the interaction that bound them.

The cosmological parameters of the models are fixed as follows: the parameters for the model (i) are chosen according to the best fit in the Planck2015 data [51]; for the model (ii) we use the results of Ref. [31], where a fit to the cosmological parameters of the model was performed using the results of WMAP7 [52]; finally, for the model (iii) we use the same parameters given by Planck2015 data for the model (i), while setting  $A$  small enough ( $A/\rho_{\text{tot0}} = 10^{-3}$ ) to ensure a good approximation to  $\Lambda$ CDM until the present time [33]. An improved analysis would incorporate in the calculations an observationally constrained value for the parameter  $A$ , obtained by constraining the homogeneous and isotropic evolution of the model using standard candles like SNeIa.

For each of the models studied, we analyse the evolution of the linear cosmological perturbations and, in particular, we compute numerically the evolution of the matter density contrast for the DM and DE components, together with the evolution of the gravitational potential. The integrations are performed from well inside the radiation era till the far future. The outcome, which we present in Fig. 1, shows that in all the models there is a very similar behaviour in the evolution of the perturbations. The largest difference seems to lie in the magnitude of DE perturbations, which can vary by up to two orders of magnitude. This fact can be explained by the sensibility of the adiabatic initial conditions, which are imposed during the radiation epoch, to small deviations in the value of the parameter of EoS of DE,  $w_d \sim -1$ . This difference in the initial values is then propagated along the whole evolution as a consequence of the linearity of the dynamical equations (3.15) and (3.16).

Using the results of the numerical integrations, we obtain for each model the theoretical prediction for the matter power spectrum, as observed today, and the late-time evolution of the observable combination  $f\sigma_8$ . In all three models the deviations of the matter power spectrum to the results of  $\Lambda$ CDM are within the  $\gtrsim 1\%$  margin, cf. Fig. 3, with the model (iii) presenting the smallest deviation. This result can be seen as a consequence of the value selected for  $A$ , which makes the LSBR model almost indistinguishable from  $\Lambda$ CDM at the background level at the present time. We compare the evolution of  $f\sigma_8$  for low redshift ( $z \lesssim 1.4$ ) with the latest observations and find that, for all the models, the curve of  $f\sigma_8$  is within the error bars for most data points. We quantify the deviation from the observations by calculating the corresponding  $\chi^2$ , which allows us to make a preliminary comparison of the results for the three models. We find that the model (ii) is the most favoured by observations. We thus conclude that although the  $\Lambda$ CDM model gives the best fit to the observations, we cannot exclude other models like the ones analysed in this work. The obtained results are in agreement with the observations and a further examination is necessary to find the footprints that can further differentiate each model. However, we stress that as we did not make an observational fit of these models (from a homogeneous and isotropic point of view and for the same set of observational data), all our results should be taken as a guideline for a more accurate study that we hope to carry in the future.

While the classical cosmological perturbations of these models at first order are well defined, as we have shown, there are still some fundamental and intrinsic problems related to phantom dark energy models. In fact, as discussed in [20], when a particle-physics description of the phantom dark energy is attempted, some instabilities may rise in the theory due to higher order effects. In the particular case of the phantom scalar field it was found that an infinite decay rate of dark energy particles into gravitons would occur unless an appropriate cut-off is introduced at some energy scale below the Planck scale, rendering the phantom scalar field as an effective description up to that energy scale. In all three models presented in this work, this kind of effects can potentially become more problematic as the Universe evolves into one of the cosmological events considered, as the energy density becomes increasingly high. Though a thorough examination of these effects and the compatibility of the phantom dark energy models with a particle physics description is outside the scope of this paper, we will take this question into account in a future work.

## ACKNOWLEDGMENTS

The authors are grateful to J. Beltrán Jiménez and V. Salzano for enlightening comments on a previous version of the paper. The work of IA is supported by a Santander-Totta fellowship “Bolsas de Investigação Faculdade de Ciências (UBI) - Santander Totta”. The work of MBL is supported by the Portuguese Agency “Fundação para a Ciência e Tecnologia” through an Investigador FCT Research contract, with reference IF/01442/2013/CP1196/CT0001. She also wishes to acknowledge the partial support from the Basque government Grant No. IT592-13 (Spain) and FONDOS FEDER under grant FIS2014-57956-P (Spanish government). This research work is partially supported by the grant UID/MAT/00212/2013. JM is thankful to UPV/EHU for a PhD fellowship and acknowledges the support from the Basque government Grant No. IT592-13 (Spain) and FONDOS FEDER, under grant FIS2014-57956-P (Spanish Government). The authors acknowledge the COST Action CA15117 (CANTATA).

### Appendix A: Decomposition of a non-adiabatic pressure

Here, we review the derivation of Eq. (3.8) which relates the pressure perturbation of a fluid  $A$  with its relative energy density perturbation and peculiar velocity. We begin by separating the pressure perturbation into its adiabatic,  $\delta p_{aA} \equiv c_{aA}^2 \delta \rho_A$ , and non-adiabatic,  $\delta p_{naA}$ , components [57]

$$\delta p_A = c_{aA}^2 \delta \rho_A + \delta p_{naA}. \quad (\text{A1})$$

Under a general gauge transformation  $(\eta, x^i) \rightarrow (\eta, x^i) + (\delta\eta, \partial^i \delta x)$  the energy density and pressure perturbations and the peculiar velocity in the final (2) and initial (1) gauges are related through [57]

$$\delta \rho_A^{(2)} = \delta \rho_A^{(1)} - \rho'_A \delta \eta, \quad \delta p_A^{(2)} = \delta p_A^{(1)} - c_{aA}^2 \rho'_A \delta \eta, \quad v_a^{(2)} + B^{(2)} = v_a^{(1)} + B^{(1)} + \delta \eta, \quad (\text{A2})$$

where  $B$  is related to the metric perturbation  $\delta g_{0i}$  and is set to zero in the Newtonian gauge [57]. From Eq. (A2) we arrive to the conclusion that the non-adiabatic term in Eq. (A1) is gauge invariant. Since by definition, we have  $\delta p_A = c_{sA}^2 \delta \rho_A$  in the rest frame of the fluid  $A$ , we can write  $\delta p_{naA}$  as [56, 57]

$$\delta p_{naA} = \delta p_A|_{\text{r.f.}} - c_{aA}^2 \delta \rho_A|_{\text{r.f.}} = (c_{sA}^2 - c_{aA}^2) \delta \rho_A|_{\text{r.f.}}. \quad (\text{A3})$$

Next, we note that in order to change from the rest frame gauge ( $v_a|_{\text{r.f.}} = 0, B|_{\text{r.f.}} = 0$ ) to the Newtonian one ( $B = 0$ ) we have to set  $v_a = \delta \eta$ , cf. Eq. (A2). Therefore, we find that in the Newtonian gauge the previous equation can be written as [56, 57]

$$\begin{aligned} \delta p_A &= c_{aA}^2 \delta \rho_A + (c_{sA}^2 - c_{aA}^2) (\delta \rho_A + \rho'_A v_A) \\ &= c_{sA}^2 \delta \rho_A - 3\mathcal{H} (c_{sA}^2 - c_{aA}^2) (1 + w_A) \rho_A v_A. \end{aligned} \quad (\text{A4})$$

### Appendix B: Classical perturbations for a Universe containing an adiabatic fluid with a negative speed of sound

On the following appendix, we remind why a universe filled with a dark energy fluid with a negative speed of sound, like it is the case of a phantom fluid with a constant equation of state, the linear perturbations of dark energy blow up. We begin by recalling the evolution equations (3.12) for the pair  $\delta_A$  and  $v_A$  in Fourier space:

$$\delta'_A = 3\mathcal{H} (w_A - c_{sA}^2) \delta_A + (1 + w_A) [9\mathcal{H}^2 (c_{sA}^2 - c_{aA}^2) + k^2] v_A + 3(1 + w_A) \Psi', \quad (\text{B1})$$

$$v'_A = (3c_{sA}^2 - 1) \mathcal{H} v_A - \frac{c_{sA}^2}{1 + w_A} \delta_A - \Psi. \quad (\text{B2})$$

We can combine these equations into a single second order inhomogeneous differential equation for  $\delta_A$  by differentiating (B1) and then using (B1) and (B2) to eliminate  $v_A$  and  $v'_A$

$$\begin{aligned} \delta''_A &+ \left[ (1 - 6w_A + 3c_{aA}^2) - \frac{\mathcal{H} (c_{sA}^2 - c_{aA}^2)' + 2\mathcal{H}' (c_{sA}^2 - c_{aA}^2)}{\mathcal{H}^2 (c_{sA}^2 - c_{aA}^2) + \frac{k^2}{9}} \right] \mathcal{H} \delta'_A \\ &- 3 \left[ \mathcal{H}' (w_A - c_{sA}^2) + \mathcal{H} (w_A - c_{sA}^2)' + \mathcal{H}^2 (1 - 3w_A) (w_A - c_{sA}^2) + 3\mathcal{H}^2 w_A (c_{aA}^2 - c_{sA}^2) \right. \\ &\quad \left. + \mathcal{H}^2 (c_{sA}^2 - w_A) \frac{\mathcal{H} (c_{sA}^2 - c_{aA}^2)' + 2\mathcal{H}' (c_{sA}^2 - c_{aA}^2)}{\mathcal{H}^2 (c_{sA}^2 - c_{aA}^2) + \frac{k^2}{9}} - \frac{k^2}{3} c_{sA}^2 \right] \delta_A \\ &= 3(1 + w_A) \left\{ \Psi'' + \left[ (1 - 3c_{sA}^2) - \frac{\mathcal{H} (c_{sA}^2 - c_{aA}^2)' + 2\mathcal{H}' (c_{sA}^2 - c_{aA}^2)}{\mathcal{H}^2 (c_{sA}^2 - c_{aA}^2) + \frac{k^2}{9}} \right] \mathcal{H} \Psi' - \left[ 3\mathcal{H}^2 (c_{sA}^2 - c_{aA}^2) + \frac{k^2}{3} \right] \Psi \right\}. \quad (\text{B3}) \end{aligned}$$

This is a wave equation with a variable damping term,  $\lambda_A$ , and mass,  $m_A$ , and with an external source,  $\mathcal{S}_A$ :

$$\delta''_A + \lambda_A \delta'_A + m_A^2 \delta_A = \mathcal{S}_A, \quad (\text{B4})$$

where

$$\begin{aligned}
\lambda_A &= \left[ (1 - 6w_A + 3c_{aA}^2) - \frac{\mathcal{H} (c_{sA}^2 - c_{aA}^2)' + 2\mathcal{H}' (c_{sA}^2 - c_{aA}^2)}{\mathcal{H}^2 (c_{sA}^2 - c_{aA}^2) + \frac{k^2}{9}} \right] \mathcal{H} \\
m_A^2 &= k^2 c_{sA}^2 - 3 \left[ \mathcal{H}' (w_A - c_{sA}^2) + \mathcal{H} (w_A - c_{sA}^2)' + \mathcal{H}^2 (1 - 3w_A) (w_A - c_{sA}^2) + 3\mathcal{H}^2 w_A (c_{aA}^2 - c_{sA}^2) \right. \\
&\quad \left. + \mathcal{H}^2 (c_{sA}^2 - w_A) \frac{\mathcal{H} (c_{sA}^2 - c_{aA}^2)' + 2\mathcal{H}' (c_{sA}^2 - c_{aA}^2)}{\mathcal{H}^2 (c_{sA}^2 - c_{aA}^2) + \frac{k^2}{9}} \right] \\
\mathcal{S}_A &= 3(1 + w_A) \left\{ \Psi'' + \left[ (1 - 3c_{sA}^2) - \frac{\mathcal{H} (c_{sA}^2 - c_{aA}^2)' + 2\mathcal{H}' (c_{sA}^2 - c_{aA}^2)}{\mathcal{H}^2 (c_{sA}^2 - c_{aA}^2) + \frac{k^2}{9}} \right] \mathcal{H} \Psi' - \left[ 3\mathcal{H}^2 (c_{sA}^2 - c_{aA}^2) + \frac{k^2}{3} \right] \Psi \right\}
\end{aligned}$$

To leading order in  $k^2$ , we have  $m_A^2 \simeq k^2 c_{sA}^2$ . Therefore, for sufficiently large  $k$ , the mass becomes imaginary if  $c_{sA}^2 < 0$  and the solutions of the homogeneous equation comprise a decaying and a growing mode, with the latter leading to the instabilities. As such, barotropic fluids with negative adiabatic squared speed of sound, for which  $c_{sA}^2 = c_{aA}^2$ , are stricken by instabilities at the linear level in perturbations. The growth of  $\delta_A$  can be particularly intense during the matter era, when most relevant modes are inside the Hubble horizon, i.e.,  $k^2 \gg \mathcal{H}^2$ , and  $\Psi \sim \text{const.}$

---

[1] A. G. Riess *et al.* [Supernova Search Team Collaboration], *Astron. J.* **116** (1998) 1009 [astro-ph/9805201].  
[2] S. Perlmutter *et al.* [Supernova Cosmology Project Collaboration], *Astrophys. J.* **517** (1999) 565 [astro-ph/9812133].  
[3] P. A. R. Ade *et al.* [Planck Collaboration], [arXiv:1502.01590 [astro-ph.CO]].  
[4] P. A. R. Ade *et al.* [Planck Collaboration], [arXiv:1502.01589 [astro-ph.CO]].  
[5] V. Sahni and A. A. Starobinsky, *Int. J. Mod. Phys. D* **9** (2000) 373 [astro-ph/9904398].  
[6] S. Weinberg, *Rev. Mod. Phys.* **61** (1989) 1.  
[7] S. M. Carroll, *Living Rev. Rel.* **4** (2001) 1 [astro-ph/0004075].  
[8] T. Padmanabhan, *Phys. Rept.* **380** (2003) 235 [hep-th/0212290].  
[9] S. Tsujikawa, [arXiv:1004.1493 [astro-ph.CO]].  
[10] K. Bamba, S. Capozziello, S. Nojiri and S. D. Odintsov, *Astrophys. Space Sci.* **342** (2012) 155 [arXiv:1205.3421 [gr-qc]].  
[11] L. Amendola and S. Tsujikawa, *Dark Energy: Theory and Observations*. First edition (Cambridge University Press, Cambridge, 2010).  
[12] S. Capozziello and V. Faraoni, *Beyond Einstein gravity: a survey of gravitational theories for cosmology and astrophysics*, vol. 170 (Springer Science & Business Media, 2011).  
[13] J. Morais, M. Bouhmadi-López and S. Capozziello, *JCAP* **1509** (2015) no.09, 041 [arXiv:1507.02623 [gr-qc]].  
[14] J. Beltrán Jiménez, R. Lazkoz, D. Sáez-Gómez and V. Salzano, [arXiv:1602.06211 [gr-qc]].  
[15] T. Abbott *et al.* [DES Collaboration], *Mon. Not. Roy. Astron. Soc.* **460** (2016) 1270 [arXiv:1601.00329 [astro-ph.CO]].  
[16] L. Amendola *et al.*, [arXiv:1606.00180 [astro-ph.CO]].  
[17] A. A. Starobinsky, *Grav. Cosmol.* **6** (2000) 157 [astro-ph/9912054].  
[18] R. R. Caldwell, *Phys. Lett. B* **545** (2002) 23 [astro-ph/9908168].  
[19] R. R. Caldwell, M. Kamionkowski and N. N. Weinberg, *Phys. Rev. Lett.* **91** (2003) 071301 [astro-ph/0302506].  
[20] S. M. Carroll, M. Hoffman and M. Trodden, *Phys. Rev. D* **68** (2003) 023509 [astro-ph/0301273].  
[21] L. P. Chimento and R. Lazkoz, *Phys. Rev. Lett.* **91** (2003) 211301 [gr-qc/0307111].  
[22] M. P. Dąbrowski, T. Stachowiak, and M. Szydłowski, *Phys. Rev. D* **68** (2003) 103519 [hep-th/0307128].  
[23] P. F. González-Díaz, *Phys. Lett. B* **586** (2004) 1 [astro-ph/0312579].  
[24] P. F. González-Díaz, *Phys. Rev. D* **69** (2004) 063522 [hep-th/0401082].  
[25] T. Ruzmaikina and A. A. Ruzmaikin, *Sov. Phys. JETP* **30** (1970) 372.  
[26] M. Bouhmadi-López, P. Chen, and Y. W. Liu, *Eur. Phys. J. C* **73** (2013) 2546 [arXiv:1302.6249 [gr-qc]].  
[27] S. 'i. Nojiri, S. D. Odintsov and S. Tsujikawa, *Phys. Rev. D* **71** (2005) 063004 [hep-th/0501025].  
[28] S. 'i. Nojiri and S. D. Odintsov, *Phys. Rev. D* **72** (2005) 023003 [hep-th/0505215].  
[29] H. Štefancić, *Phys. Rev. D* **71** (2005) 084024 [astro-ph/0411630].  
[30] M. Bouhmadi-López, *Nucl. Phys. B* **797** (2008) 78 [astro-ph/0512124].  
[31] P. H. Frampton, K. J. Ludwick and R. J. Scherrer, *Phys. Rev. D* **84** (2011) 063003 [arXiv:1106.4996 [astro-ph.CO]].  
[32] I. Brevik, E. Elizalde, S. 'i. Nojiri, and S. D. Odintsov, *Phys. Rev. D* **84** (2011) 103508 [arXiv:1107.4642 [hep-th]].  
[33] M. Bouhmadi-López, A. Errahmani, P. Martín-Moruno, T. Ouali, and Y. Tavakoli, *Int. J. Mod. Phys. D* **24** (2015) no.10, 1550078 [arXiv:1407.2446 [gr-qc]].  
[34] J. Morais, M. Bouhmadi-López, K. Sravan Kumar, J. Marto and Y. Tavakoli, [arXiv:1608.01679 [gr-qc]].  
[35] M. P. Dąbrowski, C. Kiefer, and B. Sandhöfer, *Phys. Rev. D* **74** (2006) 044022 [hep-th/0605229].  
[36] I. Albaran and M. Bouhmadi-López, *JCAP* **1508** (2015) no.08, 051 [arXiv:1505.01353 [gr-qc]].

[37] I. Albarran, M. Bouhmadi-López, F. Cabral and P. Martín-Moruno, *JCAP* **1511** (2015) no.11, 044 [arXiv:1509.07398 [gr-qc]].

[38] I. Albarran, M. Bouhmadi-López, C. Kiefer, J. Marto and P. Vargas Moniz, *Phys. Rev. D* **94** (2016) 063536 [arXiv:1604.08365 [gr-qc]].

[39] M. Bouhmadi-López and C. Y. Chen, *accepted for publication in JCAP* [arXiv:1609.00700 [gr-qc]].

[40] A. Kamenshchik, C. Kiefer and B. Sandhöfer, *Phys. Rev. D* **76** (2007) 064032 [arXiv:0705.1688 [gr-qc]].

[41] M. Bouhmadi-López, C. Kiefer, B. Sandhöfer and P. Vargas Moniz, *Phys. Rev. D* **79** (2009) 124035 [arXiv:0905.2421 [gr-qc]].

[42] A. Y. Kamenshchik and S. Manti, *Phys. Rev. D* **85** (2012) 123518 [arXiv:1202.0174 [gr-qc]].

[43] A. Y. Kamenshchik, *Class. Quant. Grav.* **30** (2013) 173001 [arXiv:1307.5623 [gr-qc]].

[44] M. Bouhmadi-López, C. Kiefer and M. Krämer, *Phys. Rev. D* **89** (2014) no.6, 064016 [arXiv:1312.5976 [gr-qc]].

[45] M. Kunz and D. Sapone, *Phys. Rev. D* **74** (2006) 123503 [astro-ph/0609040].

[46] A. Balcerzak and T. Denkiewicz, *Phys. Rev. D* **86** (2012) 023522 [arXiv:1202.3280 [astro-ph.CO]].

[47] A. V. Astashenok and S. D. Odintsov, *Phys. Lett. B* **718** (2013) 1194 [arXiv:1211.1888 [gr-qc]].

[48] T. Denkiewicz, *JCAP* **1503** (2015) 037 [arXiv:1411.6169 [astro-ph.CO]].

[49] T. Denkiewicz, [arXiv:1511.04708 [astro-ph.CO]].

[50] M. Bouhmadi-López, P. F. González-Díaz and P. Martín-Moruno, *Phys. Lett. B* **659** (2008) 1 [gr-qc/0612135].

[51] [https://wiki.cosmos.esa.int/planckpla2015/images/0/07/Params\\_table\\_2015\\_limit95.pdf](https://wiki.cosmos.esa.int/planckpla2015/images/0/07/Params_table_2015_limit95.pdf)

[52] [http://lambda.gsfc.nasa.gov/product/map/dr4/params/lcdm\\_sz\\_lens\\_wmap7\\_bao\\_h0.cfm](http://lambda.gsfc.nasa.gov/product/map/dr4/params/lcdm_sz_lens_wmap7_bao_h0.cfm)

[53] H. Kurki-Suonio *Cosmological Perturbation Theory* (lecture notes, University of Helsinki, 2003)

[54] D. Baumann *Cosmology: Part III Mathematical Tripos* (lecture notes)

[55] J. M. Bardeen, *Phys. Rev. D* **22** (1980) 1882.

[56] R. Bean and O. Dore, *Phys. Rev. D* **69** (2004) 083503 [astro-ph/0307100].

[57] J. Väliviita, E. Majerotto and R. Maartens, *JCAP* **0807** (2008) 020 [arXiv:0804.0232 [astro-ph]].

[58] C. P. Ma and E. Bertschinger, *Astrophys. J.* **455** (1995) 7 [astro-ph/9506072].

[59] G. Ballesteros and J. Lesgourgues, *JCAP* **1010** (2010) 014 [arXiv:1004.5509 [astro-ph.CO]].

[60] D. Wands and A. Slosar, *Phys. Rev. D* **79** (2009) 123507 [arXiv:0902.1084 [astro-ph.CO]].

[61] M. Bruni, R. Crittenden, K. Koyama, R. Maartens, C. Pitrou and D. Wands, *Phys. Rev. D* **85** (2012) 041301 [arXiv:1106.3999 [astro-ph.CO]].

[62] L. M. Wang and P. J. Steinhardt, *Astrophys. J.* **508** (1998) 483 [astro-ph/9804015].

[63] E. V. Linder, *Phys. Rev. D* **72** (2005) 043529 [astro-ph/0507263].

[64] E. V. Linder and R. N. Cahn, *Astropart. Phys.* **28** (2007) 481 [astro-ph/0701317].

[65] Y. S. Song and W. J. Percival, *JCAP* **0910** (2009) 004 [arXiv:0807.0810 [astro-ph]].

[66] Y. Wang *et al.*, *Mon. Not. Roy. Astron. Soc.* **409** (2010) 737 [arXiv:1006.3517 [astro-ph]].

[67] M. J. Hudson and S. J. Turnbull, *Astrophys. J.* **751** (2013) L30 [arXiv:1203.4814 [astro-ph.CO]].

[68] F. Beutler *et al.*, *Mon. Not. Roy. Astron. Soc.* **423** (2012) 3430 [arXiv:1204.4725 [astro-ph.CO]].

[69] C. Howlett, A. Ross, L. Samushia, W. Percival and M. Manera, *Mon. Not. Roy. Astron. Soc.* **449** (2015) no.1, 848 [arXiv:1409.3238 [astro-ph.CO]].

[70] W. J. Percival *et al.* [2dFGRS Collaboration], *Mon. Not. Roy. Astron. Soc.* **353** (2004) 1201 [astro-ph/0406513].

[71] C. Blake *et al.*, *Mon. Not. Roy. Astron. Soc.* **415** (2011) 2876 [arXiv:1104.2948 [astro-ph.CO]].

[72] L. Samushia, W. J. Percival and A. Raccanelli, *Mon. Not. Roy. Astron. Soc.* **420** (2012) 2102 [arXiv:1102.1014 [astro-ph.CO]].

[73] S. Satpathy *et al.* [BOSS Collaboration], [arXiv:1607.03148 [astro-ph.CO]].

[74] R. Tojeiro *et al.*, *Mon. Not. Roy. Astron. Soc.* **424** (2012) 2339 [arXiv:1203.6565 [astro-ph.CO]].

[75] H. Gil-Marn *et al.*, *Mon. Not. Roy. Astron. Soc.* **460** (2016) no.4, 4188 [arXiv:1509.06386 [astro-ph.CO]].

[76] M. Tegmark *et al.* [SDSS Collaboration], *Phys. Rev. D* **74** (2006) 123507 [astro-ph/0608632].

[77] C. Blake *et al.*, *Mon. Not. Roy. Astron. Soc.* **425** (2012) 405 [arXiv:1204.3674 [astro-ph.CO]].

[78] C. H. Chuang *et al.*, *Mon. Not. Roy. Astron. Soc.* **461** (2016) no.4, 3781 [arXiv:1312.4889 [astro-ph.CO]].

[79] L. Guzzo *et al.*, *Nature* **451** (2008) 541 [arXiv:0802.1944 [astro-ph]].

[80] S. de la Torre *et al.*, *Astron. Astrophys.* **557** (2013) A54 [arXiv:1303.2622 [astro-ph.CO]].

[81] H. Okada *et al.*, *Publ. Astron. Soc. Jap.* **68** (2016) no.33, id.47, 17 [arXiv:1504.05592 [astro-ph.GA]].

[82] E. Macaulay, I. K. Wehus and H. K. Eriksen, *Phys. Rev. Lett.* **111** (2013) no.16, 161301 [arXiv:1303.6583 [astro-ph.CO]].

[83] R. A. Battye, T. Charnock and A. Moss, *Phys. Rev. D* **91** (2015) no.10, 103508 [arXiv:1409.2769 [astro-ph.CO]].